

Yiting Xie ; Mingzhu Liang ; David F. Yankelevitz ; Claudia I. Henschke ; Anthony P. Reeves; Automated segmentation of cardiac visceral fat in low-dose non-contrast chest CT images. Proc. SPIE 9414, Medical Imaging 2015: Computer-Aided Diagnosis, 94140G (March 20, 2015);

doi:10.1117/12.2081959.

© (2015) COPYRIGHT Society of Photo-Optical Instrumentation Engineers (SPIE).
Downloading of the paper is permitted for personal use only. Systematic or multiple reproduction, duplication of any material in this paper for a fee or for commercial purposes, or modification of the content of the paper are prohibited.

Automated segmentation of cardiac visceral fat in low-dose non-contrast chest CT images

Yiting Xie^a, Mingzhu Liang^b, David F. Yankelevitz^b, Claudia I. Henschke^b and Anthony P. Reeves^a

^aSchool of Electrical and Computer Engineering, Cornell University, Ithaca, NY, USA

^bDepartment of Radiology, Icahn School of Medicine at Mount Sinai, New York, NY, USA

ABSTRACT

Cardiac visceral fat was segmented from low-dose non-contrast chest CT images using a fully automated method. Cardiac visceral fat is defined as the fatty tissues surrounding the heart region, enclosed by the lungs and posterior to the sternum. It is measured by constraining the heart region with an Anatomy Label Map that contains robust segmentations of the lungs and other major organs and estimating the fatty tissue within this region.

The algorithm was evaluated on 124 low-dose and 223 standard-dose non-contrast chest CT scans from two public datasets. Based on visual inspection, 343 cases had good cardiac visceral fat segmentation. For quantitative evaluation, manual markings of cardiac visceral fat regions were made in 3 image slices for 45 low-dose scans and the Dice similarity coefficient (DSC) was computed. The automated algorithm achieved an average DSC of 0.93. Cardiac visceral fat volume (CVFV), heart region volume (HRV) and their ratio were computed for each case. The correlation between cardiac visceral fat measurement and coronary artery and aortic calcification was also evaluated. Results indicated the automated algorithm for measuring cardiac visceral fat volume may be an alternative method to the traditional manual assessment of thoracic region fat content in the assessment of cardiovascular disease risk.

Keywords: Cardiac visceral fat, low-dose CT, computer-based segmentation, aortic calcification, coronary artery calcification.

1. INTRODUCTION

Fat in the thoracic heart region is shown to be associated with coronary calcification and various cardiovascular diseases¹⁻⁶. Manual measurement of pericardial fat from CT images is commonly used for cardiac disease risk assessment¹⁻⁶. However, in low-dose non-contrast CT images, the pericardium region is not always visible. Therefore in this study, an alternative approach is adopted to measure cardiac visceral fat. Cardiac visceral fat (CVF) is defined as fatty tissues surrounding the heart region enclosed by lungs and posterior to the sternum. Its upper limit is at the pulmonary artery level and its lower limit is the top of the diaphragm. Compared to pericardial fat, the anterior boundary of CVF is the sternum instead of the pericardium region, i.e. CVF includes pericardial fat as well as fat between the pericardium and the sternum region. It has been shown that fat in thoracic region is associated with coronary calcium^{1,4} and metabolic risk³. Therefore, CVF measurement may be useful in cardiac disease risk assessment.

The fully automated CVF algorithm employs a pre-computed anatomy label map (ALM), which contains segmentation of lungs, bony structures, aorta, and all fatty tissues within the body region. The “muscular-soft tissue” in the heart region is segmented using a rule-based approach⁷. Then the segmented heart and other organs provide a constrained region of interest for CVF, in which all the fatty tissues are extracted and measured. The CVF to heart volume ratio is also measured. For evaluation, visual inspection is first used to evaluate the overall segmentation quality. Then the automatically computed fat region is compared to manual markings in selected image slices and the Dice similarity coefficient is computed.

2. METHODS

2.1 Heart region segmentation

Robust segmentation of the mediastinum region in low-dose CT is particularly challenging because of the high levels of image noise. The muscular heart region is segmented using geometric constraints from other segmented organs⁷. It

provides a geometrically constrained region enclosed by lungs, bony structures, aorta and fatty tissues. The upper limit of this region is constrained by the location of pulmonary artery and the lower limit by the superior margin of the diaphragm, which is obtained by analyzing lung profiles¹¹. Figure 1 shows examples of heart region segmentation⁷.

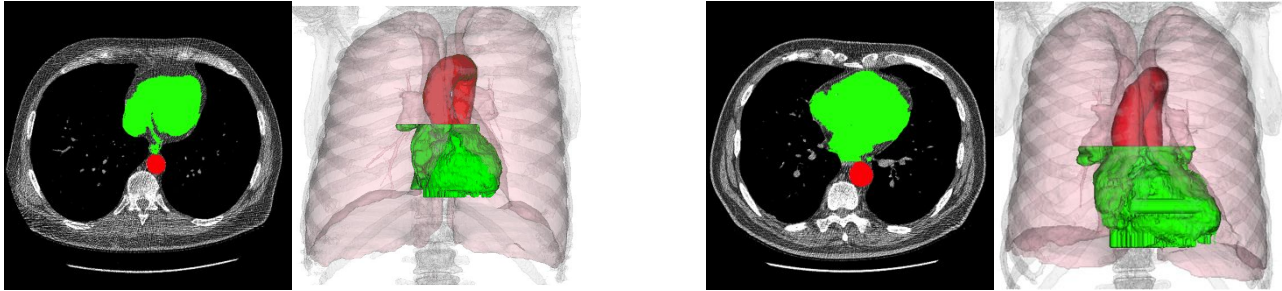


Figure 1 Two cases that demonstrate the heart region segmentation. In each case, the left image shows a 2D slice with the segmented heart (in green) and aorta (in red) overlaid on the original image and the right image shows the 3D visualization of the segmented heart (in green) together with aorta (in red) and lungs (in pink).

2.2 Cardiac visceral fat segmentation

Cardiac visceral fat (CVF) segmentation is based on the pre-segmented fatty tissues within the body region. The whole body fat segmentation employs a local noise aware algorithm designed for low-dose CT¹². Then the CVF region is modeled using the following method:

(1) Constrain the CVF region to be at the same level of the segmented heart; then use the lungs, sternum, descending aorta or vertebrae to constrain the region from left, right, anterior and posterior sides (see Figure 2 (a) and Figure 3(a)).

(2) Refine the fat region between sternum and lungs in each axial slice. If the left and right lungs are connected, eliminate all fat between sternum and lungs. Otherwise draw a horizontal line posterior to the sternum at location y_i .

Shift y_i towards the posterior region until it intersects with two lungs at location y_k , $k \leq i$. Denote the two intersection points as l_k and r_k and the distance between the two lungs as $d_k = |l_k - r_k|$.

(3) Keep shifting the horizontal line towards the posterior region until it reaches the center of the lungs at y_m . Measure two lungs' distance d_k, d_{k-1}, \dots at each location, then select y_p such that $y_p = \arg \min_p \{d_p \mid d_p = |l_p - r_p|, m \leq p \leq k\}$.

Model the fat region between sternum and lungs using a rectangular $\{left = l_p, right = r_p, anterior = y_k, posterior = y_p\}$ (see Figure 2(b) red box).

(4) Perform a connect component analysis to all the fat voxels in the constrained region. Only keep all fat voxels that are connected to the segmented heart, thus eliminating all non-cardiac fat (see Figure 2(b) red and black boxes and Figure 3 (b)).

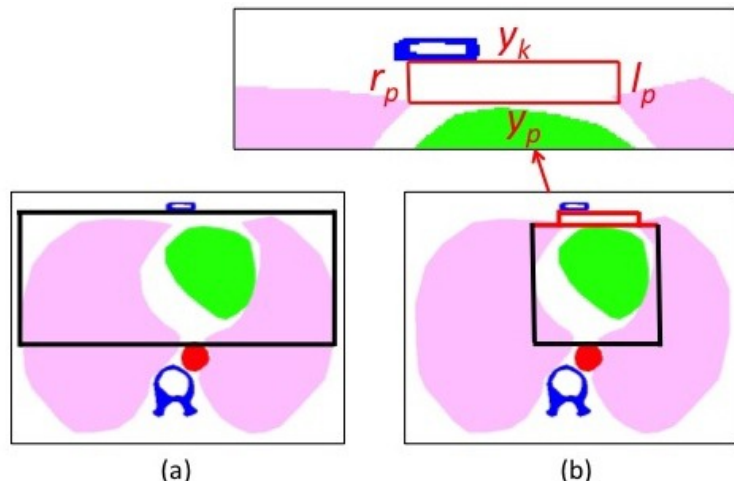


Figure 2 Illustration of CVF region in an axial slice. Fat region is modeled between sternum and lungs. From left to right: initial region (black box); final fat region with red box showing the modeled region between sternum and lungs. Together the red and black boxes show the general CVF region.

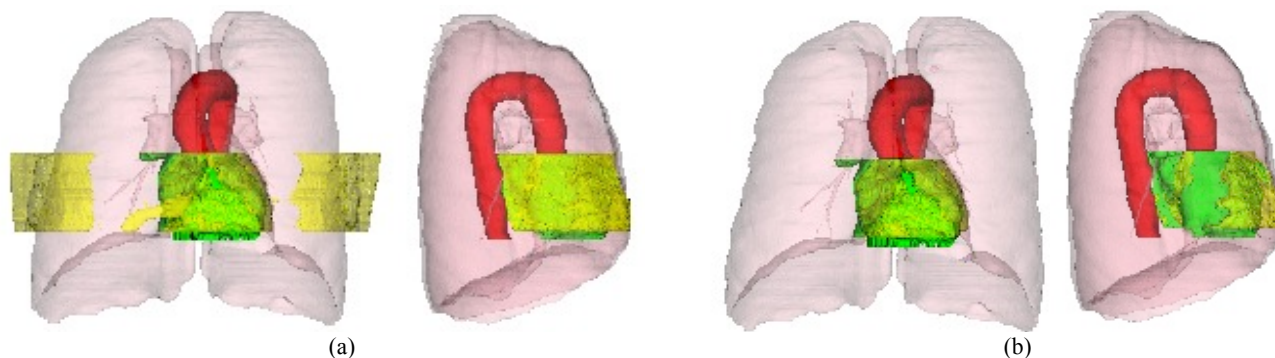


Figure 3 CVF segmentation (3D visualizations in coronal and sagittal views): (a) is the initial fat region (corresponding to Figure 2 (a)) and (b) is the final fat region (corresponding to Figure 2 (b)).

3. EXPERIMENTS

3.1 Datasets

The CVF segmentations were evaluated on 2 datasets with 347 images in total. The first is the VIA-ELCAP public dataset¹³ and contains 50 low-dose chest CT scans, among which 5 cases were excluded due to serious implant artifacts. The second dataset is the LIDC public dataset¹⁴, which contains 335 low-dose and standard-dose non-contrast CT images, among which 33 cases were excluded due to serious implants artifacts, patient prone positions, abnormal anatomical structures or excessive image noise. In total 45 low-dose scans were used from VIA-ELCAP; 79 low-dose and 223 standard-dose chest CT scans were used from LIDC. All scan images are non-contrast.

3.2 Experiments and evaluation

The CVF segmentation was evaluated both visually and quantitatively. The segmented fat was overlaid on the axial image slices and visual inspection was performed to see whether it contained significant segmentation inaccuracy. Then manual markings of an enclosed CVF region boundary were performed in 3 image slices for each case. Assuming the first and last slice containing CVF was y_1 and y_2 respectively. The 3 marked slices were located at: 10mm below y_1 ; slice at $(y_1+y_2)*0.5$; 10mm above y_2 . Ground truth fat voxels were extracted based on the markings and the Dice similarity

coefficient (DSC) between automated and manual regions was computed. The DSC is defined as twice the intersection between the automated and manual areas divided by the sum of the two areas.

In addition, the CVF volume (CVFV) and its volume to heart volume ratio (CVFV/HRV) were computed and compared to the results reported in the literature. Further the correlation of this measure with the coronary artery calcification (CAC) and aortic calcification (AC) level was assessed. CAC and AC were segmented and measured in terms of Agatston scores (AS) and volume scores (VS) using the automated methods described in our previous works^{7,15}. Correlation was computed after taking logarithm transforms of the scores and fat measurements.

4. RESULTS

Based on visual inspection, out of 347 evaluation cases, 343 cases had good CVF segmentation while 4 cases had significant over-segmentation close to diaphragm region. This was caused by the incorrect estimation of diaphragm location. Using all evaluation cases, the max, mean, minimum and standard deviation of CVF volume (CVFV) was respectively 331.70cm^3 , 103.98cm^3 , 8.62cm^3 and 63.62cm^3 . CVF to heart volume ratio (CVFV/HRV) was also computed. Its max, mean, minimum and standard deviation were respectively 1.15, 0.24, 0.01 and 0.15. Figure 4 shows example cases with different amount of CVF and Figure 5 shows the distribution of CVF and CVFV/HRV for all evaluation cases.

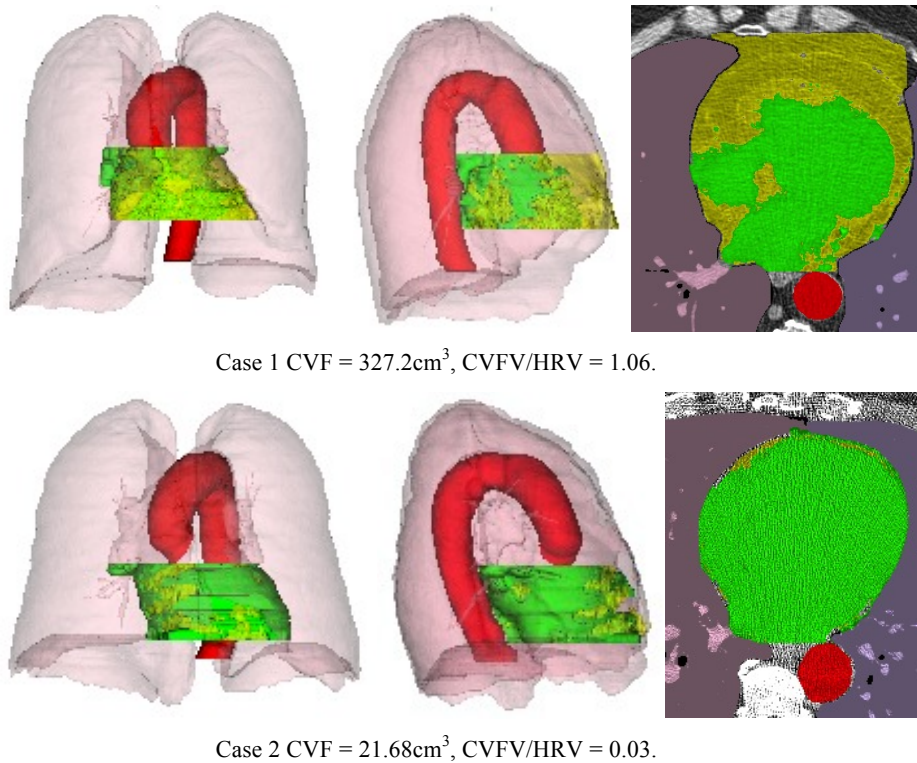


Figure 4 Example cases: case 1 had a high CVFV/HRV of 1.06 and case 2 had a low CVFV/HRV of 0.03.

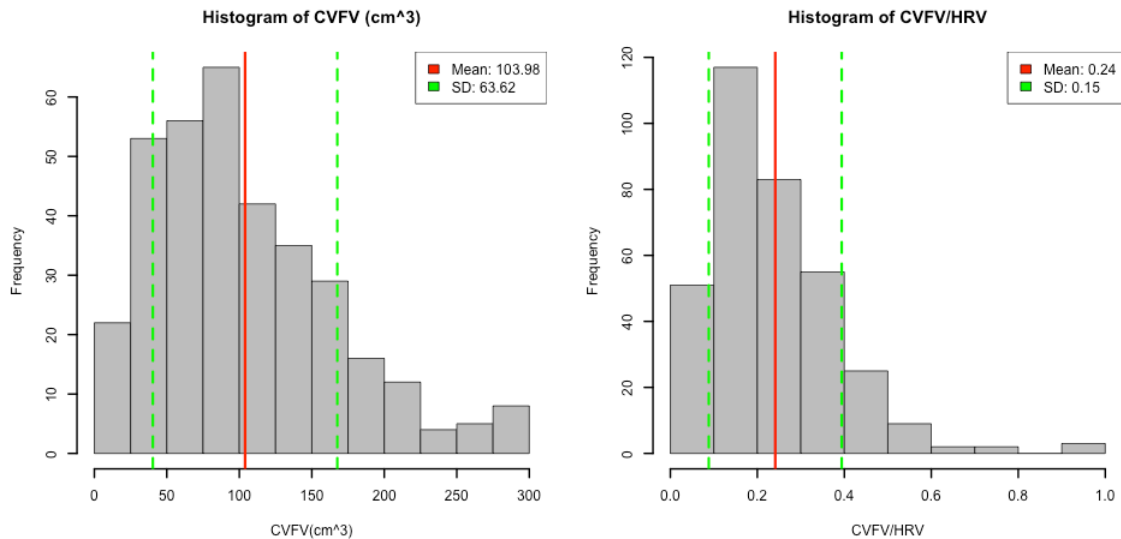


Figure 5 Histogram of CVFV and CVFV to HRV ratio.

For the 45 cases with manual markings, the mean DSC was 0.93 with a maximum of 0.99 and a minimum of 0.81. Disagreement between automated and manual segmentation usually occurred in the anterior region. The correlation of CVFV/HRV with CAC was 0.10 using the Agatston score (AS) and the volume score (VS) (p-value=0.51). The correlation of CVFV/HRV with AC was 0.25 using AS and VS (p-value=0.09). The correlation of CVFV with the AC was 0.25 using AS and VS (p-value=0.09). The CVFV was not correlated with CAC.

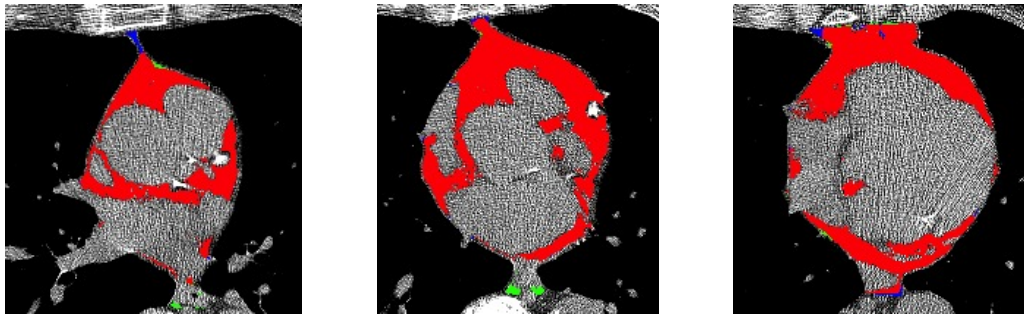
5. DISCUSSION

In general the automated algorithm performed well in the segmentation of CVF with an average DSC of 0.93. Compared to manual markings, the automated algorithm sometimes under-segmented CVF in the anterior region. Figure 6 gives 4 examples of CVF segmentation compared to manual markings. The first two examples had high DSC (0.99 and 0.95) with only slight disagreement with the manual regions. The last two examples had relatively lower DSC (0.84 and 0.81) and larger difference in the anterior regions. Two main reasons were: 1) the anterior region was modeled as a straight line in the algorithm, which was sometimes very different from the actual boundary between bony structures and soft tissues; 2) the sternum region was incorrectly estimated.

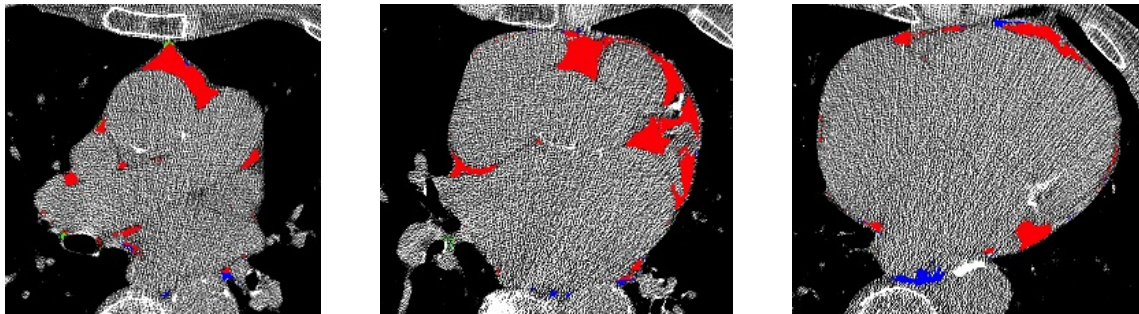
The mean CVF volume was 103.98cm^3 (standard deviation 63.62cm^3), which was smaller than the thoracic fat volume reported by Dey et al¹ and Tamarappoo et al² ($189.6 \pm 109.1\text{ cm}^3$, $196.1 \pm 82.7\text{ cm}^3$). This might be caused by the more general thoracic region defined in their works¹⁻². The mean CVFV/HRV was 0.24 (standard deviation 0.15), which was similar to the pericardiac fat to cardiac volume ratio reported by Day et al¹⁶ (0.08-0.63).

The cases with extreme fat to heart ratio ($\text{CVFV}/\text{HRV} < 0.1$ or $\text{CVFV}/\text{HRV} > 0.6$) were visually examined. It was observed that many cases with high fat to heart volume ratio ($\text{CVFV}/\text{HRV} > 0.6$) were the lung appeared to be not fully inspired or had lung region abnormalities, where the diaphragm location was very high and heart volume was significantly under-estimated. Figure 7 shows two cases with high CVFV to HRV ratio, both of which had partial lung resection, which resulted in the inaccurate estimation of diaphragm location. There was no obvious issue in cases with a low CVFV to HRV ratio.

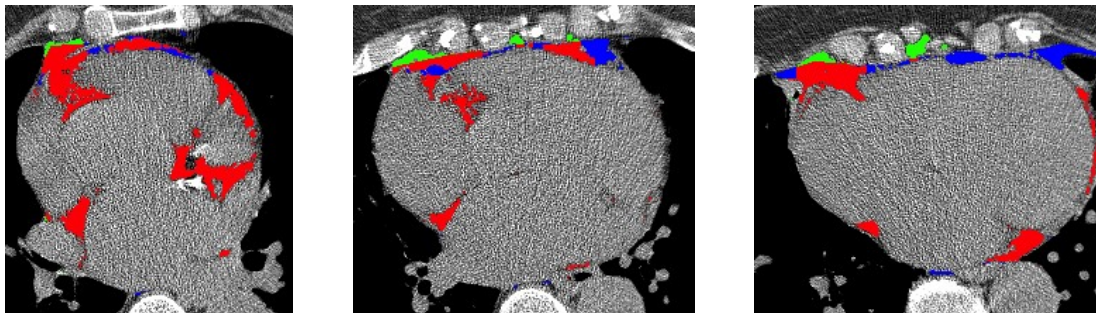
Neither CVFV or CVFV/HRV was correlated with CAC scores with statistical significance. They were both weakly correlated with the AC scores (correlation 0.25, p-value=0.09). This result was similar to what was reported by Dey et al¹, where the thoracic fat volume was 0.29 correlated with the coronary calcium score with a p-value of 0.39, and therefore not statistically significant.



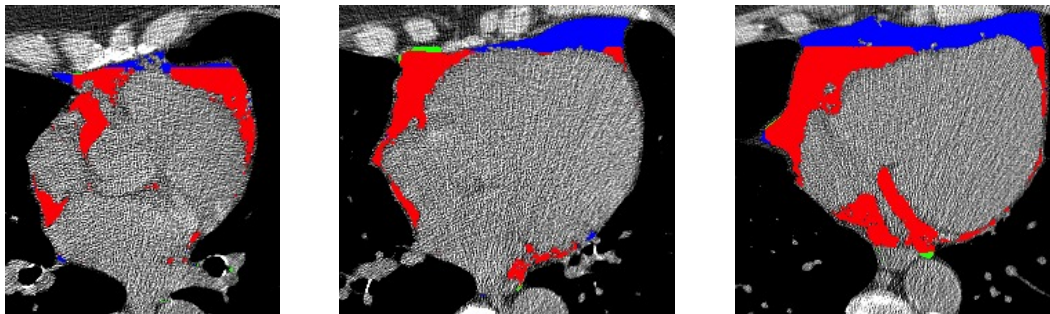
DSC = 0.99



DSC = 0.95

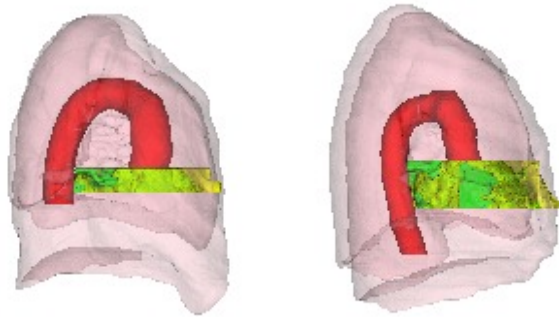


DSC = 0.84



DSC = 0.81

Figure 6 Examples showing automated CVF compared to manual markings. CVF segmentation is overlaid on the intensity images. Overlapping fat voxels are in red; fat voxels only existing in the automated segmentation are in green and fat voxels only existing in manual markings are in blue.



CVFV/HRV = 0.72

CVFV/HRV = 0.68

Figure 7 Examples cases where CVFV/HRV was likely to be overestimated due to inaccurate diaphragm location.

6. CONCLUSION

Cardiac visceral fat was automatically segmented in low-dose non-contrast chest CT scans. For the 347 low-dose and standard-dose CT scans for evaluation, 343 (98.8%) cases had good segmentation results visually. Compared to manual markings on 45 low-dose scans, the algorithm achieved an average DSC of 0.93. This indicates that the fully automated method may be a substitute for traditional manual marking assessment of cardiovascular fat.

ACKNOWLEDGMENTS

This study was supported in part by a grant from the Flight Attendant Medical Research Institute (FAMRI).

REFERENCES

- [1] Dey, D., Wong, N. D., Tamarappoo, B., Nakazato, R., Gransar, H., Cheng, V. Y., Ramesh, A., Kakadiaris, I., Germano, G., Slomka, P. J. and Berman, D. S., "Computer-aided non-contrast CT-based quantification of pericardial and thoracic fat and their associations with coronary calcium and metabolic syndrome," *Atherosclerosis*, 209 (1), 136-141 (2010).
- [2] Tamarappoo, B., Dey, D., Shmilovich, H., Nakazato, R., Gransar, H., Cheng, V. Y., Friedman, J. D., Hayes, S. W., Thomson, L. E., Slomka, P. J., Rozanski, A. and Berman, D. S., "Increased Pericardial Fat Volume Measured From Noncontrast CT Predicts Myocardial Ischemia by SPECT," *JACC: Cardiovascular Imaging*, 3 (11), 1104-1112 (2010).
- [3] Thanassoulis, G., Massaro, J. M., Hoffmann, U., Mahabadi, A. A., Vasan, R. S., O'Donnell C. J. and Fox C. S., "Prevalence, Distribution, and Risk Factor Correlates of High Pericardial and Intrathoracic Fat Depots in the Framingham Heart Study," *Circulation: Cardiovascular Imaging*, 3 (5), 559-566 (2010).
- [4] Rosito, G. A., Massaro, J. M., Hoffmann, U., Ruberg, F. L., Mahabadi, A. A., Vasan, R. S., O'Donnell, C. J. and Fox, C. S., "Pericardial Fat, Visceral Abdominal Fat, Cardiovascular Disease Risk Factors, and Vascular Calcification in a Community-Based Sample: The Framingham Heart Study," *Circulation*, 117 (5), 605-613 (2008).
- [5] Ding, J., Hsu, F. C., Harris, T. B., Liu, Y., Kritchevsky, S. B., Szklo, M., Ouyang P., Espeland, M. A., Lohman, K. K., Criqui, M. H., Allison, M., Bluemke, D. A. and Carr, J. J., "The association of pericardial fat with incident coronary heart disease: the Multi-Ethnic Study of Atherosclerosis (MESA)," *Am J Clin Nutr.* 90 (3), 499-504 (2009).
- [6] Taguchi, R., Takasu, J., Itani, Y., Yamamoto, R., Yokoyama, K., Watanabe, S. and Masuda, Y., "Pericardial fat accumulation in men as a risk factor for coronary artery disease," *Atherosclerosis*, 157 (1), 203-209 (2001).

- [7] Xie, Y., Cham, M. D., Henschke, C., Yankelevitz, D. and Reeves, A. P., "Automated coronary artery calcification detection on low-dose chest CT images," Proc. SPIE Medical Imaging 9035, 90350F (2014).
- [8] Dey, D., Ramesh, A., Slomka, P. J., Nakazato, R., Cheng, V. Y., Germano, G. and Berman, D. S., "Automated algorithm for atlas-based segmentation of the heart and pericardium from non-contrast CT," Proc. SPIE 7623, 762337 (2010).
- [9] Ding, X., Terzopoulos, D., Diaz-Zamudio, M., Berman, D. S., Slomka, P. J. and Dey, D., "Automated Epicardial Fat Volume Quantification from Non-contrast CT," Proc. SPIE Medical Imaging 9034, 90340I (2014).
- [10] Yalamanchili, R., Dey, D., Kurkure, U., Nakazato, R., Berman, D. S. and Kakadiaris, I. A., "Knowledge-based Quantification of Pericardial Fat in Non-Contrast CT Data," Proc. SPIE Medical Imaging 7623, 76231X (2010).
- [11] Reeves, A. P., Biancardi, A. M., Yankelevitz, D. F., Cham, M. D. and Henschke, C. I., "Heart region segmentation from low-dose CT scans: an anatomy based approach," Proc. SPIE Medical Imaging 8314, 83142A (2012).
- [12] Padgett, J., Biancardi, A. M., Henschke, C. I., Yankelevitz, D. and Reeves, A. P., "Local noise estimation in low-dose chest CT images," Int J CARS 9, 221-229 (2014).
- [13] VIA-ELCAP Public Lung Image Database, <http://www.via.cornell.edu/databases/lungdb.html> (18 December 2014).
- [14] Armato, S. G. 3rd, McLennan, G., Bidaut, L., McNitt-Gray, M. F., Meyer, C. R., Reeves, A. P., Zhao, B., Aberle, D. R., Henschke, C. I., Hoffman, E. A., Kazerooni, E. A., MacMahon, H., Van Beeke, E. J., Yankelevitz, D., Biancardi, A. M., Bland, P. H., Brown, M. S., Engelmann, R. M., Laderach, G. E., Max, D., Pais, R. C., Qing, D. P., Roberts, R. Y., Smith, A. R., Starkey, A., Batrah, P., Caligiuri, P., Farooqi, A., Gladish, G. W., Jude, C. M., Munden, R. F., Petkovska, I., Quint, L. E., Schwartz, L. H., Sundaram, B., Dodd, L. E., Fenimore, C., Gur, D., Petrick, N., Freymann, J., Kirby, J., Hughes, B., Castele, A. V., Gupte, S., Sallamm, M., Heath, M. D., Kuhn, M. H., Dharaiya, E., Burns, R., Fryd, D. S., Salganicoff, M., Anand, V., Shreter, U., Vastagh, S., Croft, B. Y., "The Lung Image Database Consortium (LIDC) and Image Database Resource Initiative (IDRI): A Completed Reference Database of Lung Nodules on CT Scans," Medical Physics, 38(2), 915-931 (2011).
- [15] Xie, Y., Htwe, Y. M., Padgett, J., Henschke, C., Yankelevitz, D. and Reeves, A. P., "Automated aortic calcification detection in low-dose chest CT images," Proc. SPIE Medical Imaging 9035, 90350P (2014).
- [16] Dey, D., Suzuki, Y., Suzuki, S., Ohba, M., Slomka, P. J., Polk, D., Shaw, L. J., Berman, D. S., "Automated Quantitation of Pericardiac Fat From Noncontrast CT," Investigative Radiology, 43 (2): 145-153 (2007).